Journal of ELECTRONIC MATERIALS
https://doi.org/10.1007/s11664-021-08836-5

ORIGINAL RESEARCH ARTICLE

A Composition-Dependent Unified Analytical Model for Quaternary InAlGaN/GaN HEMTs for pH Sensing

KAVITA THORAT UPADHYAY[1,2,4] and MANJU K. CHATTOPADHYAY[3,5]

1.—Department of Electronics and Communication Engineering, Institute of Engineering and Science, IPS Academy, Indore, M.P. 452012, India. 2.—Department of Electronics and Telecommunication Engineering, Institute of Engineering and Technology, Devi Ahilya University, Indore, (M.P.) 452017, India. 3.—School of Electronics, Devi Ahilya University, Khandwa Road, Indore, M.P. 452017, India. 4.—e-mail: kavita.thorat@gmail.com. 5.—e-mail: mkorwal@yahoo.com

Group III–V material alloys such as gallium nitride (GaN) with piezoelectric and pyroelectric properties are used for designing advanced devices suitable for harsh surroundings such as high temperature and acidic ambience. In the present paper, we introduce a unified model using InAlGaN quaternary alloy in the barrier layer to analyze the performance of pH sensors based on high electron-mobility transistors (HEMTs) Our model is used to accurately calculate the threshold voltage, the sheet charge concentration and thus the drain current, in response to changes in the pH values of the electrolyte put in the gate area of the InAlGaN/GaN heterostructure based sensor. We have taken three devices for our studies with varying In mole fraction from 0% to 16% and Al mole fraction from 23% to 74%. The sensitivity of a HEMT based pH sensor depends on its transconductance. The maximum transconductance values of the InAlGaN/GaN devices were found to be much higher than those of the AlGaN/GaN HEMT devices. A theoretical sensitivity of 1.3 mA/pH was achieved for the quaternary structures. Our model shows good agreement with the experimental data available in literature, presenting less than 1.2% root mean square error in almost all the devices. We observe that HEMTs based on the InAlGaN/GaN structures have better sensitivity than the AlGaN/GaN structures in pH sensing applications. Our findings may be used in designing quaternary HEMT based novel pH sensors.

Key words: Analytical model, quaternary alloy, HEMTs, PH sensors, InAlGaN, sensitivity

INTRODUCTION

In the present-day world, all types of biological and chemical process involved in agriculture, industrial -drugs, semiconductors, textiles, food, consumer goods, and healthcare depend on the right pH levels.[1] Supervision and control of the pH level is important for preventing unwanted chemical reactions and for optimizing desired reactions. Additionally, accurate measurement of the pH levels is essential in the study of wastewater and waste products discharged from chemical industries, in ascertaining the strength of concrete structure[2] and absorption of nutrients from the soil,[3] in food spoilage monitoring, in the study of tissue metabolism,[4] in cancer diagnostics, and so forth.[5] The pH of body fluids is also an indicator of a disease. The normal pH values for human blood and sweat are 7.35–7.45 and 4–6.8, respectively. Reliable measurement of cellular activity, genome sequencing and enzyme activity in the blood require high pH sensitivity in devices used for measurement.[6]

Numerous efforts have been made in the past towards device development of various pH sensors.

(Received June 20, 2020; accepted February 23, 2021)

Published online: 22 March 2021

They include micro-cantilevers, ion sensitive field effect transistor (ISFET) technology, thin-film technology (TFT), glass membrane pH electrodes, fiber-optic pH sensors, and potentiometric pH sensors.[7,8] While all these sensors have their own specific characteristics, no single sensor has all the required advanced features of high sensitivity, high measurement precision, cost effectiveness, miniaturization and ease of mass production.[9]

Lately, the group III-V semiconductors based high electron mobility transistors (HEMTs) are being explored as suitable candidates for pH sensing. Properties of the gallium nitride (GaN) material devices such as the wide band gap, compatibility with high-temperature environment, strong chemical stability and good biological suitability make them interesting sensor materials.[10] Unlike the sensors based on conventional semiconductors, the layers in GaN based HEMTs are undoped. Spontaneous and piezoelectric polarization in GaN HEMTs create a two-dimensional electron gas (2DEG) channel which balances the charges on the surface and increases the ambience sensitivity towards the surrounding gases, bio-chemicals and solutions with varying pH levels. Additionally, this 2DEG channel removes the necessity of an add-on sensor membrane, thus reducing the cost further.

Because of biocompatibility and stable chemical properties, AlGaN and InGaN are also important candidates for performance enhancement of pH sensors. These materials also have large sheet carrier concentration, a wide band gap and a higher sensitivity for harsh environments like high temperature and acidic or alkaline solutions.[11]

A number of researchers have experimentally investigated the response of AlGaN/GaN HEMTs to polar liquids and their pH sensing characteristics.[9,12–16] Lattice mismatch in the AlGaN/GaN devices create an inverse polarization effect which tends to degrade the device performance. One can overcome this problem by employing better lattice matched AlInN/GaN heterostructure.[17] A higher 2DEG density can be achieved at lower thickness of AlInN barrier layer than that of the AlGaN layer. However, due to clustering and high immiscibility between InN and AlN, the development of AlInN has its limitations.

The quaternary compound InAlGaN has been studied as a new barrier layer in the HEMTs to overcome the problems of lattice mismatch and immiscibility in the alloys.[18,19] Quaternary InAlGaN films deliver all degrees of freedom essential to independently alter the bandgap, lattice parameter and polarization. Noteworthy enhancement in electron mobility has been achieved in InAlGaN/GaN heterostructures by numerous authors by adding a small quantity of Ga in the AlInN alloys.[18–25] The first study of InAlGaN was reported in 1996 for performance in RF[20,21] Ketteniss et al.[22] explored the performance of the InAlGaN/GaN HEMTs with variations in the physical parameters. Hwang et al.[23] and Dogmus et al.[24] verified the charge transport properties of InAlGaN. Ravi et al.[25] recently studied the structural and optical properties of InAlGaN/GaN epilayers. $In_{0.1}Al_{0.65–0.7}Ga_{0.25–0.2}N$/GaN heterostructures result in the highest thermodynamically stable states within the calculated composition range and, therefore, exhibit significant improvement in terms of electron mobility.[17] This heterostructure thus has recently experienced a renewed interest in reduction-based applications, solar blind UV detectors and molecule detectors.[26]

There have been few attempts reported in the literature to model the conduct of the GaN-based chemical sensors.[27,28] Bayer et al. modeled the GaN/AlGaN/GaN/Ga_2O_3 based chemical sensors by using the equilibrium reaction rate as a control parameter to match the experimental data.[27] Sciullo et al. modeled the contact of the AlGaN/GaN-based chemical sensors with the electrolyte by tuning the reaction rates and the density of the reactive surface sites to obtain a symmetric response within the pH range 1–10.[28] However, they ignored the surface oxide. Rabbaa et al. also studied the charging mechanism of the GaN-based chemical sensor.[29] Anvari et al. presented a theoretical study of various factors affecting the charging mechanism and characteristics of the Ga_2O_3/GaN/AlGaN based ISFET by using a triple layer model (TLM).[30]

However, all these reports are focused on the AlGaN/GaN based materials systems. To the best of our knowledge, no work has been reported yet on the quaternary InAlGaN/GaN HEMTs for pH sensing applications. Very few mathematical models are found in the literature to analyze the characteristics of the InAlGaN/GaN HEMTs with respect to other physical properties.[31–34] In our previous work, we illustrated a charge based analytical model for the I_d-V_d characteristics of the InAlGaN/GaN HEMTs.[35] The present study aims to provide an insight into the performance of the quaternary InAlGaN heterostructures, specifically as a pH sensor. We explore the physical factors that control the performance and sensitivity of the InAlGaN-based sensors depending on their structural parameters. We also compare various design parameters, viz., changes in the threshold voltage, transconductance and sensitivity of the InAlGaN/GaN and AlGaN/GaN materials systems. Additionally, we find an optimized In and Al mole fraction composition for the best pH specific sensitivity.

This paper is organized as follows: The details of the device structure under study are given in "Device Structure" section. Charge-based current model and the equations for surface potential are presented in "Model Description" section. Our computational results for various devices are discussed in "Results and Discussion" section. The conclusions are presented in "Conclusion" section.

DEVICE STRUCTURE

Parish et al. stated that the nonlinear pH response of the AlGaN-surface devices can be avoided by employing a reference electrode based sensor configuration. For AlGaN/GaN-based chemical sensors operated with a reference electrode, a linear response to the pH value is achieved by varying the potential applied to the electrolyte gate. If the AlGaN/GaN based sensing systems are employed in an application for which the use of a reference electrode is not feasible, a linear pH response demands the use of GaN capped heterostructures.[36] It is worthwhile to note that the GaN HEMT based sensors are normally on devices, and hence, the reference electrode may be eliminated for the miniaturization of the sensing device and to eliminate the reliability issues.[37] Murugapandiyan et al. highlighted that a 1-nm AlN spacer layer with wide band gap characteristics can surmount the scattering effects of the device to confine more electrons in the 2DEG and can thus alleviate the gate leakage current effects.[38]

The cross-sectional view of the HEMT device in Fig. 1 depicts a quaternary InAlGaN barrier layer on a GaN buffer layer. A reference electrode is used to apply gate bias at the open gate area. Electrolytic pH solution is assumed to be filled between the gate area and the electrode.

Figure 2 shows the energy band diagram of our quaternary device. A 2DEG channel is formed in the GaN layer of the HEMT due to the spontaneous and piezoelectric polarization at the interface.

MODEL DESCRIPTION

It is already well known that the development of a 2DEG in the heterostructure is a very significant application of the polarization property of the nitride alloys. Few extrapolations from theoretical and experimental work on the polarization property of quaternary InAlGaN alloys are available in the literature.[31,32] In Ref. 35, we studied the structural and electronic properties of quaternary alloy InAlGaN, by using interpolation model based on the Vegard's law. Accordingly, the threshold voltage V_{th} in HEMTs is related to the polarization as

$$V_{\text{th}} = \frac{\emptyset_b}{q} - \frac{\Delta E_c}{q} - \frac{qn_d d^2}{2\varepsilon} - \frac{q\sigma_{\text{int}} d}{\varepsilon} \quad (1)$$

where $\emptyset_b, \Delta E_c, q$ and n_d are the height of the Schottky barrier, the conduction band discontinuity, electronic charge and doping concentration, respectively, while, ε is the permittivity of the material, d is the thickness of the InAlGaN layer, $\sigma_{\text{int}} = P_{\text{GaN}} - P_{\text{InAlGaN}}$, P_{GaN} is the polarization of GaN and P_{InAlGaN} is the polarization of InAlGaN obtained by the addition of spontaneous and piezoelectric polarizations as

$$P_{\text{InAlGaN}} = P_{\text{sp}}(\text{InAlGaN}) + P_{\text{pz}}(\text{InAlGaN}) \quad (2)$$

Carrier Density Model

The sheet charge density n_s of the 2DEG as a function of the position x in the channel can be obtained by solving the one-dimensional Poisson's equation and is given as[29]:

$$n_s = \frac{\varepsilon}{qd}\left(V_g - V_{th} - V_y - \frac{E_F}{q}\right) \quad (3)$$

Here, V_g, V_y and E_F are the gate voltage, the channel potential at a distance y and the Fermi level, respectively.

Here, we extend our model in Ref. 35 for calculating the threshold voltage and the transfer characteristics of the quaternary InAlGaN device as a function of varying pH levels. We are analyzing a model for the pH sensors operating in the region

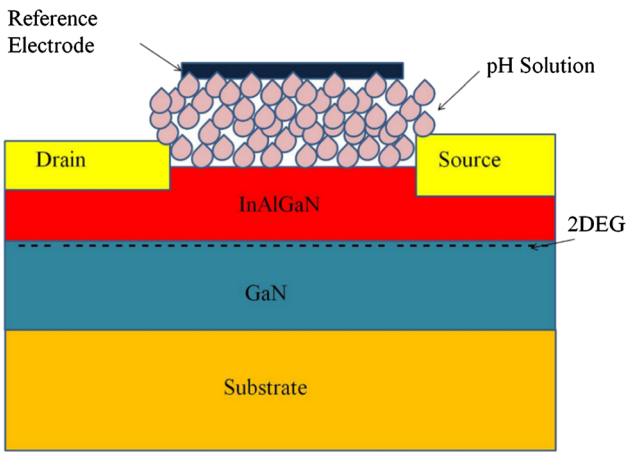

Fig. 1. Depiction of the device structure of quaternary alloy InAlGaN/GaN HEMT with 2DEG formed in the channel. The pH solution is assumed to be present in the conventional gate area.

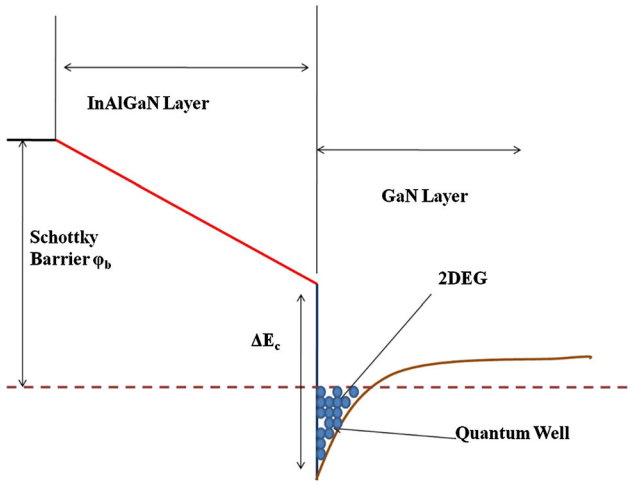

Fig. 2. Energy band diagram of the InAlGaN/GaN HEMT. ΔE_c is the difference in conduction band energies of the InAlGaN and GaN layers.

with $E_F < E_c$. In this region the carrier concentration in the InAlGaN barrier layer (n_B) is negligible.[39] Hence, we diligently ignore n_B and use only n_s in our model by modifying it for the quaternary InAlGaN materials system by choosing suitable material specific design parameters. Our parameters are, therefore, different from those used in Swamy's model for AlGaN/GaN HEMTs.[39] Thus, we have

$$n_s = \frac{AV_{\mathrm{go}}}{(1+B)}\left(\frac{1-A^{\frac{2}{3}}\gamma_0}{(1+B)^{\frac{2}{3}}V_{\mathrm{go}}^{\frac{1}{3}}}\right) \tag{4}$$

where V_{go}= V_g-V_{th}, A = ε/qd, B = A/qD, D is the density of states and γ_0 is a constant estimated from Shubnikov-de Haas or cyclotron resonance experiments.

Charge-Based Drain Current Model

An analytical model for current is formulated using the definition of the drain current along the channel given by

$$I_D = q\mu W\left[n_T\left(\frac{\mathrm{d}V_y}{\mathrm{d}y}\right) - \left(\frac{kT}{q}\right)\left(\frac{\mathrm{d}n_T}{\mathrm{d}y}\right)\right] \tag{5}$$

$$dV_y = -dn_T\left(\frac{A+D}{AD} + \frac{2}{3}\gamma_0 n_T^{\frac{-1}{3}}\right) \tag{6}$$

where W is the width, μ is the low field mobility of the device, n_T is the sheet carrier density in the channel that contributes to current conduction at any given distance y, k is the Boltzmann constant and T is the ambient temperature. Taking the limit of y from source S to drain D, and integrating Eq. 5, we get the expression for the drain current as

$$I_D = \frac{q\mu_{eff}W}{L}\left[\frac{A+D}{2AD}\left(n_s^2 - n_D^2\right) + \frac{2}{5}\gamma_0\left(n_s^{\frac{5}{3}} - n_D^{\frac{5}{3}}\right) + \frac{kT}{q}\left(n_s - n_D\right)\right] \tag{7}$$

Here, n_s and n_D are the charge carrier concentrations at the source and drain, respectively. μ_{eff} is the effective 2DEG mobility and L is the gate length. n_s here is calculated using Eq. 4. The calculation of n_D is explained in the next section.

Saturation Voltage

A relationship commonly used in many MOSFET models, has been adopted in the present work for the case of HEMTs to get the saturation voltage and effective mobility, respectively, as follows[39]

$$V_{Sat} = \frac{v_s V_{go}}{v_s + \frac{\mu_{eff}V_{go}}{2L}} \tag{8}$$

$$\mu_{eff} = \frac{\mu_0}{\left(1 + p_1 V_{go} + p_2 V_{go}^2\right)\left(1 + p_3 V_{ds}\right)} \tag{9}$$

Here, v_s is the saturation velocity and p_1, p_2 and p_3 are the fitting parameters.

Once the saturation voltage is calculated, we obtain the effective drain voltage V_{effD}. The calculation of V_{effD} is intended to give a smooth transition between the applied drain-source voltage V_{ds} and the saturation voltage V_{sat}[40]

$$V_{effD} = V_{sat}\left[1 - \frac{\ln\left[1 + exp\left(1 - \alpha\frac{V'_{ds}}{V_{sat}}\right)\right]}{\ln(1+e)}\right] \tag{10}$$

Here α is the transition width parameter and V'_{ds} represents the effective drain-source voltage for the channel. It is calculated by subtracting the voltage drops due to the resistances at the source and drain from the drain-source voltage. The charge carrier concentration at the drain n_D, is calculated using Eq. 4 by replacing V_{go} with V_{gdo}= V_{go}− V_{effD}.

pH Sensing

Researchers have put substantial effort into identifying the sensing mechanism of metal oxides (MO_x) based pH sensors. Generally, when the sensor is exposed to a solution, the MO_x layer is covered by hydroxide groups due to dissociative adsorption of water. The oxide sites formed by releasing protons cause a potential difference between the sensing electrode and the reference electrode. As per site-binding theory, surface groups –O–, –OH and $–OH_2^+$ are formed after the immersion of the sensor in an aqueous solution.[1] Hydroxide ions and protons from the solution are attracted to the surface cations and to the oxygen ions from the MO_x layer, respectively. Consequently, the MO_x are covered by hydroxide groups. The generated MO_x groups can donate a proton to the solution and form a negative surface group or accept a proton from the solution converting into a positive surface group.[1] A deviation in the pH value of a solution affects the balanced state of the MO_x layer. This can cause changes in electrical properties and surface potential of the surface electrode. The surface potential at the sensing layer and electrolyte interface is determined by the number of binding sites on the sensing membrane. The surface potential is used to derive the concentration of the H^+ ions in the solution.

When the surface of a HEMT is exposed to an electrolyte solution with a specific concentration, the variation in the surface charge and the potential causes a variation in the effective threshold voltage of the device. This causes the modulation of the drain current. This mechanism is used to build a sensor for the measurement of the pH level of the solution.

The effect of the presence of electrolyte solution appears in terms of the potential,[41] expressed mathematically as:

$$\psi_0 = -\log_e 10\delta_t V_{th}(pH - pH_{pzc}) \quad (11)$$

where $\delta_t = \frac{\gamma}{1+\gamma}$, $\gamma = \frac{qN_{ss}\eta}{C_{eq}V_{th}}$, $\eta = 2*10^{-\frac{(pK_b - pK_a)}{2}}$, $C_{eq} = \frac{C_{DL}C_{stern}}{C_{DL}+C_{stern}}$, $C_{DL} = \frac{\sqrt{8\varepsilon V_T q n_0}}{2V_{th}}$, $pH_{pzc} = \frac{pK_a + pK_b}{2}$, γ is defined by Gouy–Chapman stern model parameter, C_{stern} is the capacitance of the stern layer (C_{stern} = 20 μF/cm^2), C_{DL} is a double layer capacitance derived from the Gouy–Chapman–Stern model, n_0 is the ionic charge concentration in the electrolyte, V_T is the thermal voltage and N_{ss} is the site binding charge at the interface of electrolyte solution and gate oxide layer which can be determine by the site-binding model, pH_{pzc} is the pH of the pristine point of zero charge, pK_a and pK_b are the equilibrium protonation constants of the surface.[30]

It has been observed that a thin unintentional Ga_2O_3 layer is formed on the exposed GaN (or AlGaN or InAlGaN) surface when it comes into contact with the air.[29] The properties of the Ga_2O_3 layer are either like a native oxide formed on the surface of the device when exposed to air or water or like that of a thicker layered oxide that is developed thermally on the surface. We have assumed that the quaternary InAlGaN layer in our HEMT also gets covered with a thin layer of Ga_2O_3. This unintentionally formed Ga_2O_3 layer brings change in the surface potential. Table I shows the site-binding model parameter of Ga_2O_3 oxide layer. We observe that there is no concurrence in the literature on the protonation rates at the Ga_2O_3/ solution interface. Various studies have reported different values of pH_{pzc}, e.g., 7, 8.47 and 9.[42,43] The value used by us i.e. $pH_{pzc} = 7.86$ falls very much within this range.

The surface potential ψ_0 is subtracted from the threshold voltage represented by Eq. 1 to get the effective threshold voltage. Thus, the potential change with pH value of the solution is coupled to the 2DEG concentration n_s in the HEMT channel to change the source-drain current, described by Eq. 3.

RESULTS AND DISCUSSION

I-V Characteristics of Devices

Referring to the literature, the quaternary InAlGaN barrier layers for HFET device applications are found to have two major alloy compositions. One (generally below 20%) incorporates Ga in the lattice-matched InAlN barrier layer to improve the crystalline quality and the other (generally below 10%) incorporates In in the AlGaN barrier layer for small in-plane strain.[34] Therefore we use device structures similar to the ones used in references[14] and[22] to validate our theoretical calculations. All the device dimensions and fitting parameters are summarized in Table II.

Table I. Site-binding parameters of passivation layers[30]

Passivation Layer	ε	pK_a	pK_b	N_{ss}
Ga_2O_3	10.2	4.81	10.91	3x10^{14} cm^{-2}

Figure 3 shows the threshold voltage of the devices by altering the pH levels for the experimental device reported by Kokawa et al.[14]. Device A has gate length L = 10 μm, width W = 500 μm, thickness of quaternary InAlGaN layer d = 22 nm with varying Al and In mole fractions. Variation in Al and In mole fractions brings a corresponding deviation in the parameters such as the dielectric constant, the polarization and the band gap of the semiconductor. This deviation is then reflected in the variation of the threshold voltage of the device. In Fig. 3, we observe that the results of our model at 0% In and 23% Al mole fractions, matched closely with the experimental data reported by Kokawa et al.[14] for AlGaN/GaN HEMT. We also infer that by increasing the mole fraction of Al from 0.33 to 0.38 and keeping the In fraction constant at 0.05, the threshold voltage of the device decreases and shifts towards a negative value. Our model was further applied to the Device B, Device C and Device D reported by Ketteniss et al.[22] With the higher mole fraction of In, the threshold voltage of the devices shifted more towards the negative value.

The gate leakage characteristics of the open-gate AlGaN/GaN devices were experimentally studied by Kokawa et al.[14] They inferred that the open-gate HEMT produces negligibly low gate currents in the solution under dark conditions. Their results indicated that the effects of gate leakage on the potential-control of the solution/AlGaN interfaces thus could be ignored. We thus have not incorporated the gate leakage associated with our pH sensor in the computations.

Figure 4 shows the variation in the threshold voltage with respect to pH for the same device structures, as taken in Fig. 3. The maximum observed variation is 60 mV/pH for the different device structures used here. The average sensitivity is 58.5 mV/pH, which is approximately equal to the Nernstian response, i.e. 58.9 mV/pH. Kokawa et al.[14] reported an experimental pH sensitivity of 57.5 mV/pH. It is also observed here, that the variation is higher for pH $<$ 7, i.e. acidic solutions and lesser for the basic solutions.

Figure 5 shows the composition dependent variation of the threshold voltage as a function of pH for the device with structure parameters W = 100 μm, L = 1 μm and d = 13.5 nm. It is inferred that the change in mole fractions of Al and In do not affect the sensitivity of the threshold voltage.

Figure 6 shows the transfer characteristics of Device A HEMT for different mole fractions of Al and In, when put in an electrolyte solution with the pH level of 4. With 0% of In and 23% of Al mole fractions, the calculated values of the drain current matched well with the experimental data reported by Kokawa et al.[14] Similarly, Figs. 7 and 8 show the

Table II. Model and device parameters

	Parameters			
	Device A In_yAl_x-$Ga_{1-x-y}N$	**Device B $In_{0.16}$-$Al_{0.74}Ga_{0.10}N$**	**Device C $In_{0.15}$-$Al_{0.7}Ga_{0.15}N$**	**Device D $In_{0.14}$-$Al_{0.66}Ga_{0.20}N$**
Depicted In	Figures 3, 6-8,11	Figures 3,9	Figures 3,10	Figure 3
Al mole fraction in InAlGaN (Unitless)	Variable	0.74	0.7	0.66
In mole fraction in InAlGaN (Unitless)	Variable	0.16	0.15	0.14
InAlGaN layer Thickness (nm)	22	13.5	12.8	11.3
Gate length L (μm)	10	1	1	1
Gate width W (μm)	500	100	100	100
Low field mobility μ_0 (cm^2/V-s)	950	1740	1790	1750
Fitting parameter p_1 (1/Volt)	− 0.875	− 0.073	− 0.081	− 0.001
Fitting parameter p_2 (1/$Volt^2$)	0.28	0.073	0.075	0.12
Fitting parameter p_3 (1/Volt)	0.65	0.07	0.081	0.02
Source-gate region resistance R_s(Ohm)	0.2	0.6	0.6	0.6
Drain-gate region resistance R_d (Ohm)	0.2	0.6	0.6	0.6
α, transition width parameter (unitless)	0.23	0.85	0.9	0.95

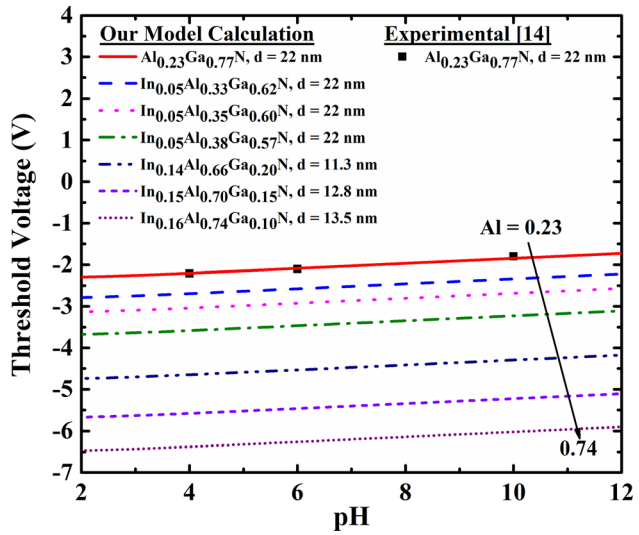

Fig. 3. Threshold voltage of the device with varying pH level of the electrolyte solution.

transfer characteristics with pH = 6 and pH = 10 electrolyte solutions, respectively.

We validate our model by comparing our calculated results with the I-V characteristics of InAlGaN/GaN HEMTs fabricated and reported by Ketteniss et al.[22] when there is no electrolyte solution in the gate area. For comparison, we have considered two devices: Device B and Device C. Various device parameters of the structures are summarized in Table II. Figures 9 and 10 show the respective transfer characteristics of Device B and Device C when they are put in the electrolyte solution with pH level 2, 4 and 12 at a drain-source voltage of 10 V. A reduction in the drain current and a positive shift in the threshold voltage have been observed when the pH level rises above 2. Moreover, we see that there is a change in the threshold voltage when the gate area of the device is exposed to air and when the electrolyte solution with certain pH value is filled in the gate area. This change may be attributed to the varying surface potential of the electrolyte solution for different pH level.

Figure 11 shows the change in drain current as a function of pH. To validate our model, we have taken the experimental data reported by Kokawa et al.[14], they have reported the drain current of the $Al_{0.23}Ga_{0.77}N$/GaN based Device A with thickness of the barrier layer d = 22 nm, at V_g= − 0.5 V and V_d = 0.2 V. The sensitivity for the drain current alteration with the pH is calculated as 56.79 μA/pH for the AlGaN/GaN device. The drain current of device is calculated by reducing its barrier thickness to d = 15 nm at the same V_d = 0.2 V and V_g = − 0.5 V. The current reduces by about 62.4%, and the sensitivity decreases to 49.46 μA/pH. We tried to find out the current at d = 12 nm for $Al_{0.23}Ga_{0.77}N$ by increasing the drain voltage to 5 V. However, no proper output

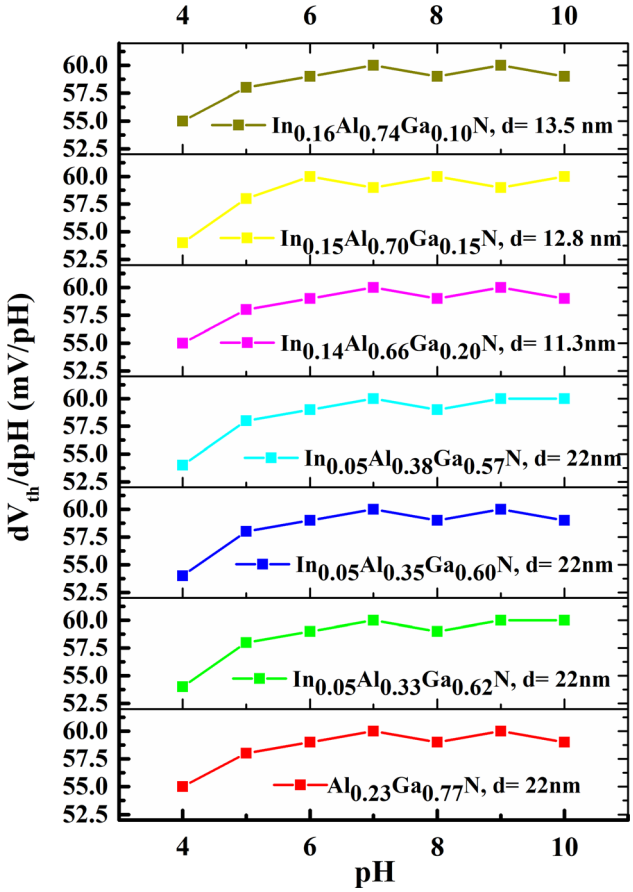

Fig. 4. Variation of the threshold Voltage/pH with the pH values for different device structures. Threshold voltage variation in all the devices is nearly equal to the Nernstian response of 58.9 mV/pH.

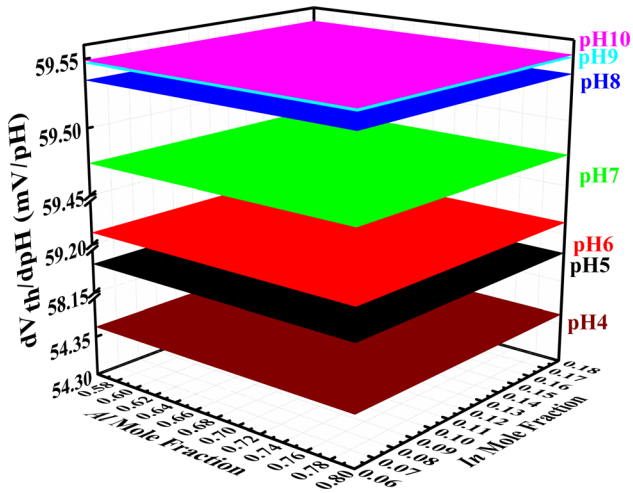

Fig. 5. Variation dV_{th}/dpH for at various mole fraction of Al and In, for W = 100 μm, L = 1 μm, d = 12 *nm*.

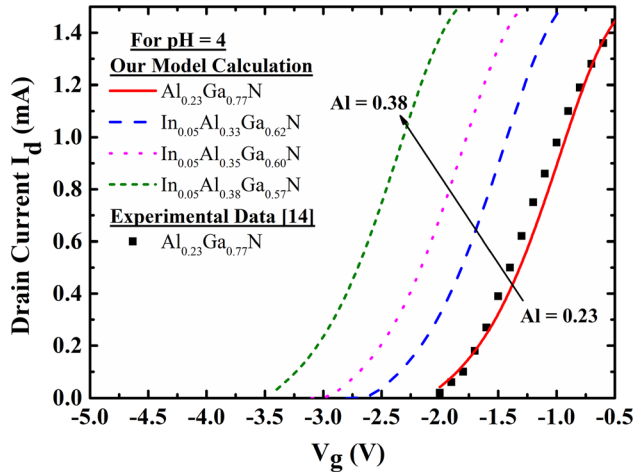

Fig. 6. Drain current versus gate voltage of device for different Al and In mole fractions in a solution with pH = 4.

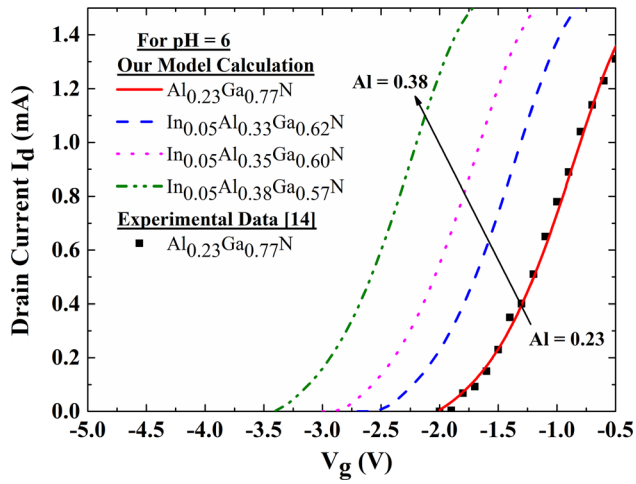

Fig. 7. Drain current versus gate voltage of devices with different Al and In mole fractions in a solution with pH = 6.

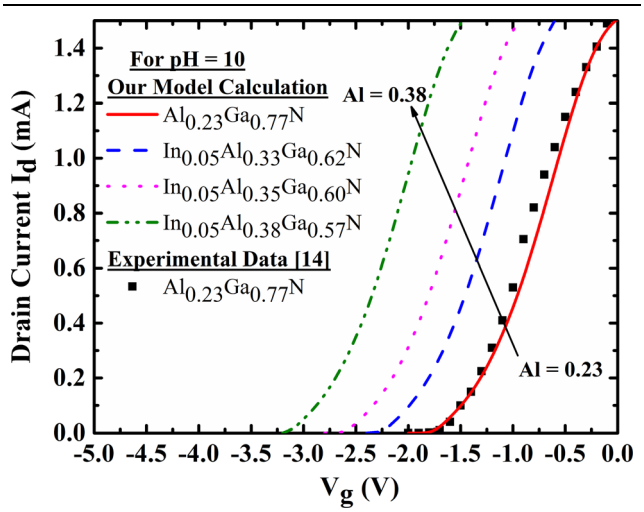

Fig. 8. Drain current versus gate voltage of devices with different Al and In mole fractions in a solution with pH = 10.

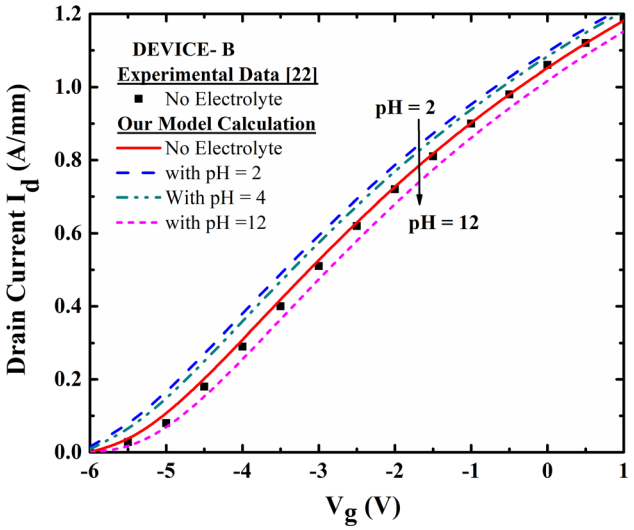

Fig. 9. Drain current versus gate voltage of devices at different pH values. The experimental data is taken from Ref. 22.

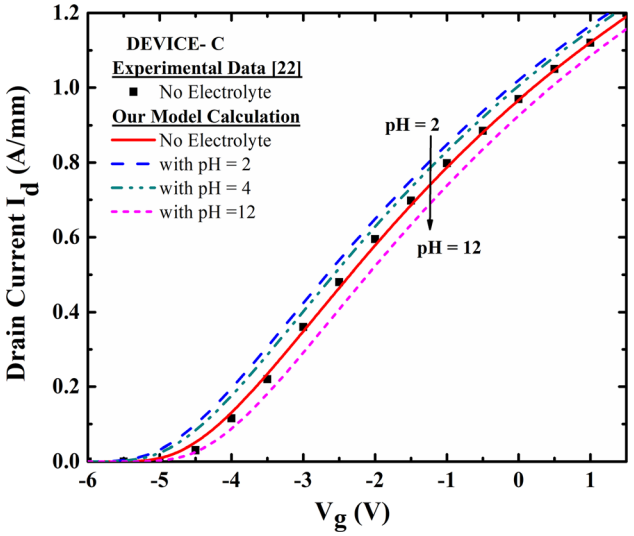

Fig. 10. Drain current versus gate voltage of Device C for different pH values.

was obtained in this case. The probable reason may be a layer breakdown due to lattice mismatch.

Changing the Al mole fractions to 0.28 and 0.33 leads to an output at d= 12 nm. With an $Al_{0.28}Ga_{0.72}N$/GaN barrier layer, we find that the drain current is slightly higher than that of $Al_{0.23}Ga_{0.77}N$ with same barrier thickness of d = 12 nm. For $Al_{0.33}Ga_{0.67}N$, with d = 12 nm at V_d = 5 V, the drain current increases considerably and the sensitivity increases to 0.21 mA/pH. By using the quaternary alloy in the pH sensor, the drain current increases from a range of 26 μA-1.5 mA to 80–113 mA for a lattice matched thin barrier layer. For $In_{0.14}Al_{0.66}Ga_{0.20}N$, with d = 12 nm at V_d = 5 V, the maximum drain current increases to 91 mA, while the sensitivity increases to 1.1 mA/pH. For $In_{0.15}Al_{0.70}Ga_{0.15}N$, with d = 12 nm at V_d = 5 V, the maximum drain current increases to 107 mA,

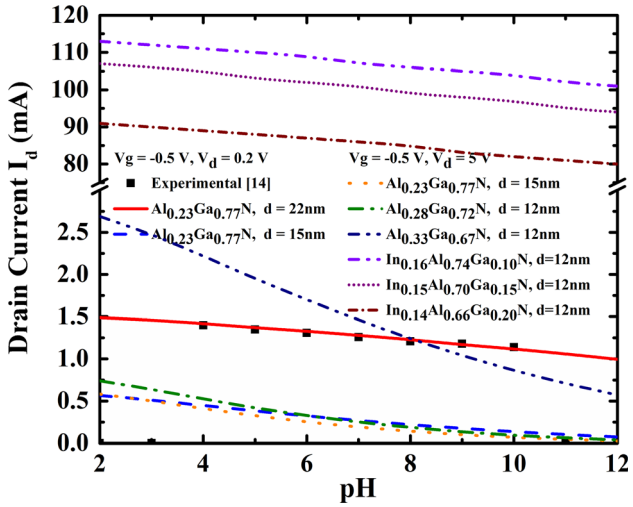

Fig. 11. Sensitivity, i.e. change in the drain current with alteration in pH level for the HEMT devices based on AlGaN/GaN structure and the InAlGaN/GaN structure.

while the sensitivity increases to 1.3 mA/pH. For $In_{0.16}Al_{0.74}Ga_{0.10}N$, with d = 12 nm at V_d = 5 V the maximum drain current and sensitivity are 113 mA and 1.2 mA/pH respectively.

To find the accuracy of our mathematical model with the experimental data, we calculated the root mean square error (RMSE), the mean absolute error (MAE) and the normalized RMSE (NRMSE) and summarized them in Table III.

pH Sensing Response of the HEMT Devices

The sensitivity of the HEMT based pH sensor is defined as the change of I_d in response to the unit change of the pH in the solution at a constant drain voltage V_d.[37,44]

$$\text{Sensitivity} = \frac{\Delta I_d}{\Delta pH} = \frac{\Delta I_d}{\Delta V_g} \times \frac{\Delta V_g}{\Delta pH} = g_m \times S_v \quad (12)$$

While g_m is the transconductance determined by the characteristics of the HEMT device,S_v is the surface sensitivity determined by the characteristics of the gate surface material. The variation of pH in the solution causes a potential variation on the gate surface and g_m amplifies this variation. Therefore, g_m is an important parameter for studying the current sensitivity of the pH sensors.

The parameter $\Delta I_d = I_d(\text{pH}) - I_d(\text{pH=7})$ is defined as the change in the I_d of the device at different values of pH with respect to the I_d of the device at pH=7.[17] As shown in Fig. 12a, the maximum variation of drain current I_d of Device A ($Al_{0.23}Ga_{0.77}N$/GaN structure with barrier layer thickness d = 22 nm), at V_g = – 0.5 V and V_d = 0.2 V is as small as 0.28 mA. Similarly, for $Al_{0.23}Ga_{0.77}N$/GaN, d = 15 nm, V_g = – 0.5 V, V_d = 0.2 V and 5 V, the maximum change in current are obtained as 0.3 mA and 0.39 mA, respectively, with

Table III. Root mean square error (RMSE), mean absolute error (MAE) and normalized root mean square (NRMSE) for the model calculations and the experimental data

Device	Error in model calculation w.r.t. experimental result	RMSE	MAE	NRMSE
Device A $Al_{0.23}Ga_{0.77}N$	Threshold voltage at different pH level[14]	0.029	0.023	0.014
	Drain current I_d at pH = 4[14]	$6.23416*10^{-05}$	0.049	0.079
	Drain current I_d at pH = 6[14]	$2.88504*10^{-05}$	0.023	0.044
	Drain current I_d at pH = 10[14]	$6.49454*10^{-05}$	0.047	0.093
Device B In0.16Al0.74Ga0.10N	Drain current I_d with no pH electrolyte[22]	0.011274677	0.01	0.02
Device C $In_{0.15}Al_{0.7}Ga_{0.15}N$	Drain current I_d with no pH electrolyte[22]	0.008798331	0.009	0.017

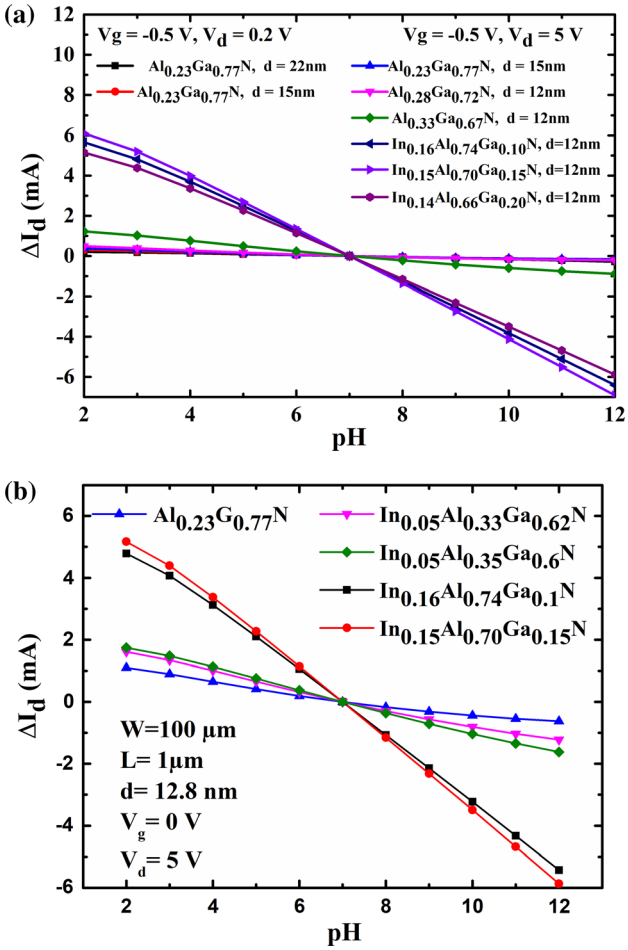

Fig. 12. (a) Variation of I_d with the pH value with respect to I_d (pH=7). (b) Variation of I_d with yhe pH value with respect to I_d (pH=7) for devices with the same physical dimensions but with different Al and In mole fractions.

respect to the current at pH = 7. When the mole fraction of Al increases to 0.28, (d = 12 nm, V_g = − 0.5 V, V_d = 5 V) the maximum change in the current is 0.49 mA for pH = 2 w.r.t. pH = 7. For the ternary alloy $Al_{0.33}Ga_{0.67}N$/GaN (d = 12 nm at V_d = 5 V), the sensitivity increases to 1.23 mA for pH = 2 w.r.t. pH = 7. When we analyze the change in current in the quaternary alloy HEMT, the sensitivity for the devices with $In_{0.14}Al_{0.66}Ga_{0.20}N$, $In_{0.15}Al_{0.7}Ga_{0.15}N$ and $In_{0.16}Al_{0.74}Ga_{0.10}N$ barrier layers with d = 12 nm, V_g = − 0.5 V, V_d = 5 V at pH = 2 with respect to pH = 7, increases to 5.15 mA, 6.107 mA and 5.66 mA, respectively. It is observed that the HEMTs sustain a linear relationship between ΔI_d and the pH value.

To study ΔI_d versus pH behavior at similar device dimensions and biasing conditions, we plot Fig. 12b for W = 100 μm, L = 1 μm, d = 12.8 nm. It is observed from Fig. 10b, that under similar biasing conditions and with the similar physical dimensions, sensitivity of the device changes with the change in In and Al mole fractions. Also, increase in In mole fraction increases the sensitivity up to a particular level only.

Figure 13a shows the transconductance g_m of Device A, which was reported by Kokawa et al.[14], as mentioned earlier, the device has L = 10 μm, W = 500 μm with $Al_{0.23}Ga_{0.77}N$ barrier layer thickness d = 22 nm at V_d = 0.2 V. The calculated maximum transconductance $g_{m,\max}$ of the device is 1.36 mS at pH = 10, 4 and 2. When we reduce the thickness of barrier layer to d = 12 nm, while keeping all other parameters same, we cannot find the complete response of the device. Therefore, we increase the mole fraction of Al to 0.33. The transfer characteristics thus obtained along with the g_m, are plotted in Fig. 13b at V_d = 0.2 V. The $g_{m,\max}$ calculated here is 2.06 mS. To increase the output current and g_m, the applied gate voltage is increased to V_d = 5 V. This increased the $g_{m,\max}$ value to 5.05 mS as shown in Fig. 13c. When the barrier layer is changed from ternary AlGaN alloy to InAlGaN with mole fractions In = 0.15 and Al = 0.70, the g_m increases to 26 mS, as can be seen in Fig. 13d. It can be observed that by keeping same device dimensions, i.e. L = 10 μm, W = 500 μm, d = 12 nm and changing the material of barrier layer from ternary $Al_{0.33}Ga_{0.67}N$ to

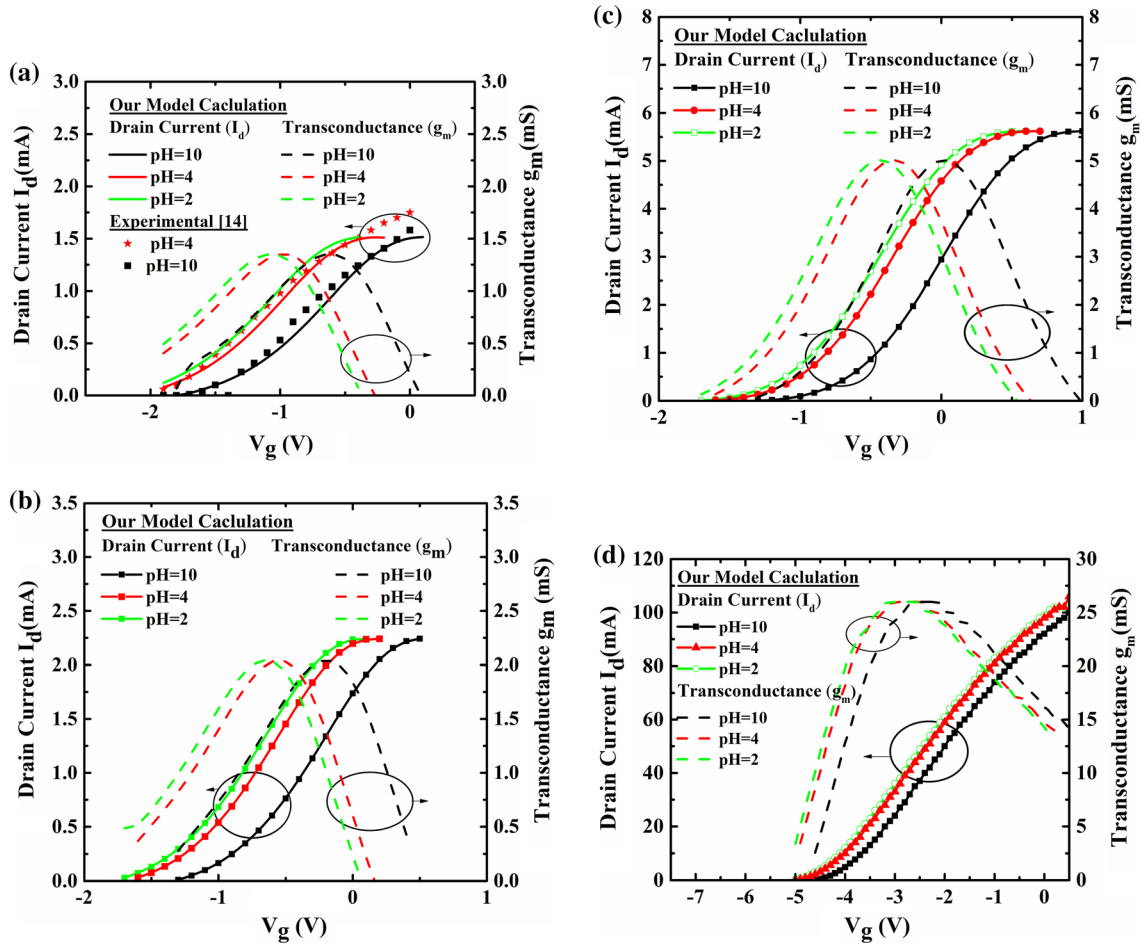

Fig. 13. (a) Transfer characteristics and transconductance g_m of Device A with $Al_{0.23}Ga_{0.77}N$ barrier layer thickness d = 22 nm, L = 10 μm, W = 500 μm at V_d = 0.2 V. (b): Transfer characteristics and transconductance g_m of the device with $Al_{0.33}Ga_{0.77}N$ barrier layer thickness d= 12 nm, L = 10 μm, W = 500 μm at V_d = 0.2 V. (c): Transfer characteristics and transconductance g_m of the device with $Al_{0.33}Ga_{0.77}N$ barrier layer thickness d = 12 nm, L = 10 μm, W = 500 μm at V_d = 5 V. (d) Transfer characteristics and transconductance g_m of the device with $In_{0.15}Al_{0.70}Ga_{0.15}N$ barrier layer thickness d = 12 nm, L = 10 μm, W = 500 μm at V_d = 5 V.

quaternary $In_{0.15}Al_{0.70}Ga_{0.66}N$ alloy, the g_m increases by an order of magnitude.

Figures 14 and 15 depict the variation of I_d and g_m with V_g at different physical dimensions and mole fractions, respectively. We calculated the transconductance for the devices experimentally reported by Kettenis et al.[22]. The results are shown in Fig. 14a, b and c. Figure 14a shows the g_m of Device B ($In_{0.16}Al_{0.74}Ga_{0.10}N$, d = 13.5 nm, L = 1 μm, W = 100 μm, V_d = 5 V). The $g_{m,\max}$ is calculated as 25 mS. Figure 14b shows the g_m of Device C ($In_{0.15}Al_{0.70}Ga_{0.15}N$, d = 12.8 nm, L = 1 μm, W = 100 μm, V_d = 5 V). The $g_{m,\max}$ of Device C is calculated as 26 mS. Figure 14c shows the g_m of Device D ($In_{0.14}Al_{0.66}Ga_{0.20}N$, d = 11.3 nm, L = 1 μm, W = 100 μm, V_d = 5 V). The $g_{m,\max}$ of Device D is calculated as 25 mS too.

To observe the actual parameters which affect the sensitivity of the device, we have calculated the transconductance by keeping all device dimensions same but only changing the mole fraction of In and Al in barrier layers, This is plotted in Fig. 15. The dimensions are: L = 1 μm, W = 100 μm, thickness of barrier layer d = 12 nm, and V_d = 5 V. The Fig. 15a, b, c and d depict that the $g_{m,\max}$ for $In_{0.16}Al_{0.74}Ga_{0.10}N$, $In_{0.15}Al_{0.70}Ga_{0.15}N$ and $In_{0.14}Ga_{0.66}Ga_{0.20}N$ are calculated as 27 mS, 28 mS and 26 mS, respectively.

In our calculations, we have not taken into consideration the impact of packaging of the sensor. Practically, the sensor must have a packaging to protect and physically separate the chip metallization from the liquid. To realize this, considerable separation is kept between the sensing region and the input-output area using long connecting wires. These wires introduce large series resistance, R_{sr}. The R_{sr} is negligible in conventional GaN power HEMTs since the power device is directly mounted on the PCB board in a compact packaging, thus their g_m is directly proportional to the W/L ratio. Conversely, the sensitivity of the sensor packaging depends on the R_{sr} and thus the sensitivity may not

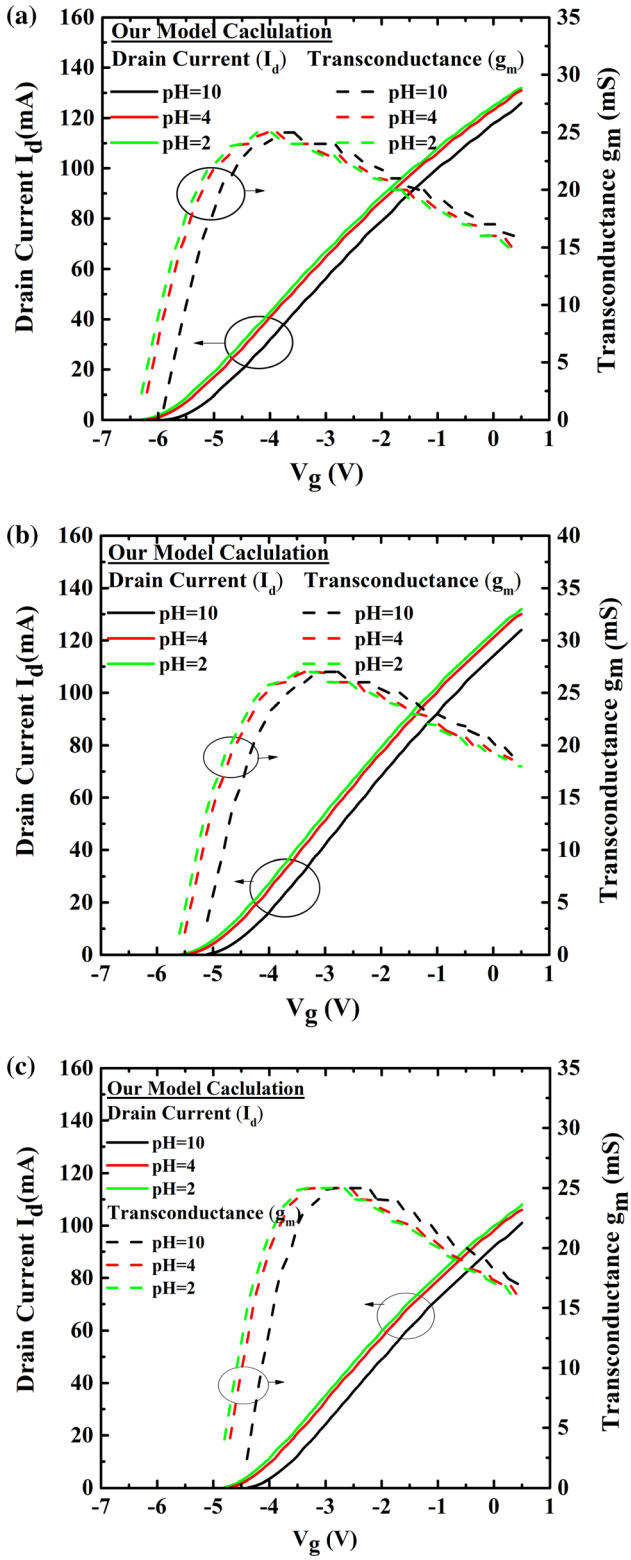

Fig. 14. (a) Transfer characteristics and transconductance g_m of the device with $In_{0.16}Al_{0.74}Ga_{0.10}N$ barrier layer thickness d = 13.5 nm, L = 1 μm, W = 100 μm at V_d = 5 V. (b) Transfer characteristics and transconductance $g_m$of the device with $In_{0.15}Al_{0.7}Ga_{0.15}N$ barrier layer thickness d = 12.8 nm, L = 1 μm, W = 100 μm at V_d = 5 V. (c) Transfer characteristics and transconductance g_m of device with barrier layer $In_{0.14}Al_{0.66}Ga_{0.10}N$, d = 11.3 nm, L = 1 μm, W = 100 μm at V_d = 5 V.

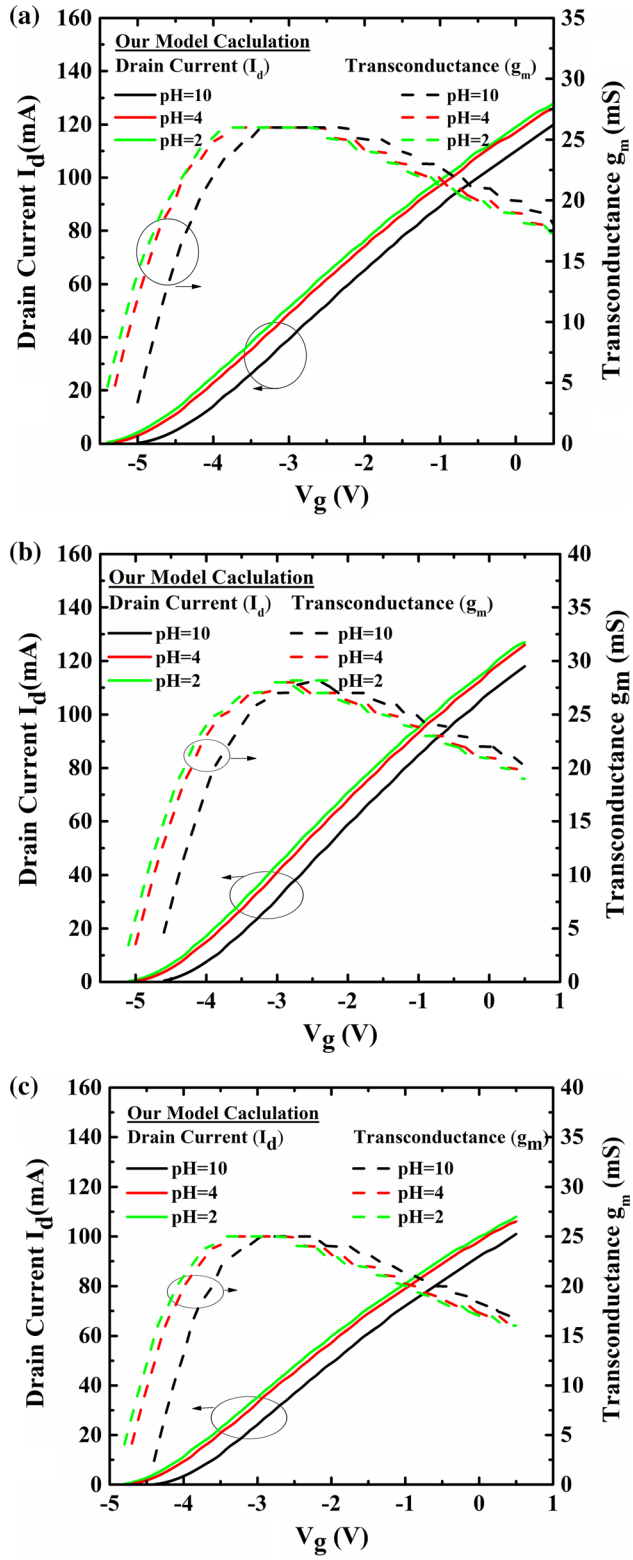

Fig. 15. (a) Transfer characteristics and transconductance $g_m$of the device with barrier layer $In_{0.16}Al_{0.74}Ga_{0.10}N$ thickness 12 nm, L = 1 μm, W = 100 μm at V_d = 5 V. (b) Transfer characteristics and transconductance g_m of the device with barrier layer $In_{0.15}Al_{0.70}Ga_{0.15}N$, d = 12 nm, L = 1 μm, W = 100 μm, V_d = 5 V. (c) Transfer characteristics and transconductance g_m of the device with barrier layer $In_{0.14}Ga_{0.66}Ga_{0.20}N$, d = 12 nm, L = 1 μm, W = 100 μm, V_d = 5 V.

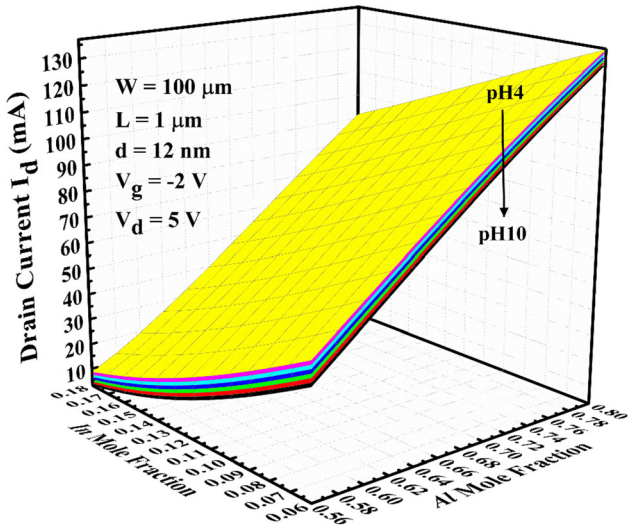

Fig. 16. Drain current I_d with constant device structure d = 12 nm, L = 1 μm, W = 100 μm, V_d = 5 V, V_g = − 2 V for variable composition of Al and In.

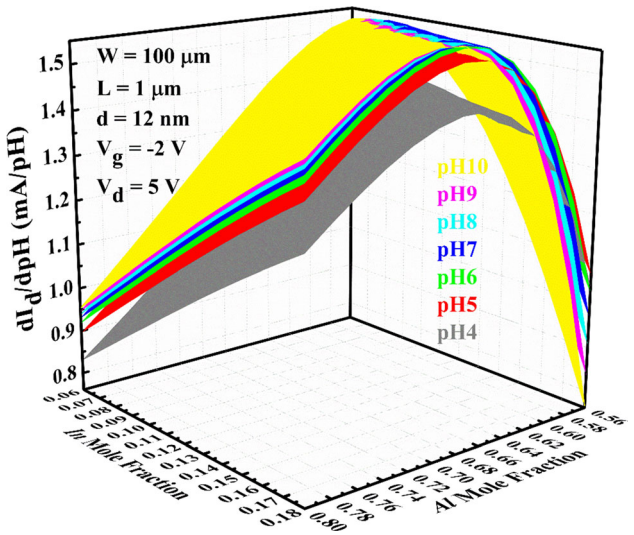

Fig. 17. Sensitivity dI_d/dpH versus Al and In mole fractions for W = 100 μm, L = 1 μm, d = 12 nm, V_g = − 2 V and V_d = 5 V.

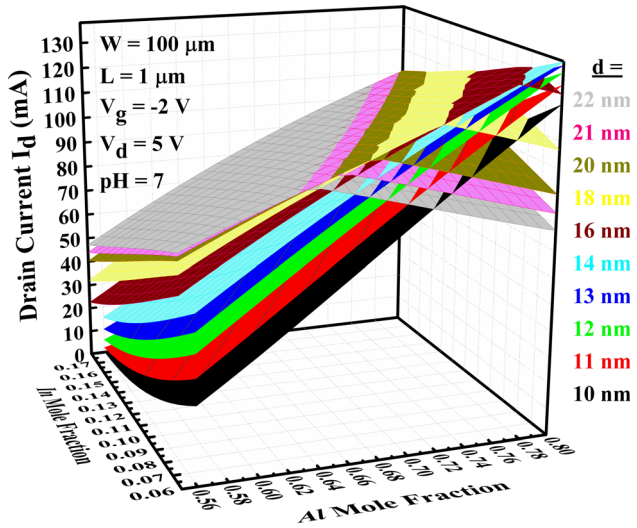

Fig. 18. Drain Current I_d with constant device structure L = 1 μm, W = 100 μm, V_d = 5 V, V_g = − 2 V and at variable composition of Al, In and barrier thickness d.

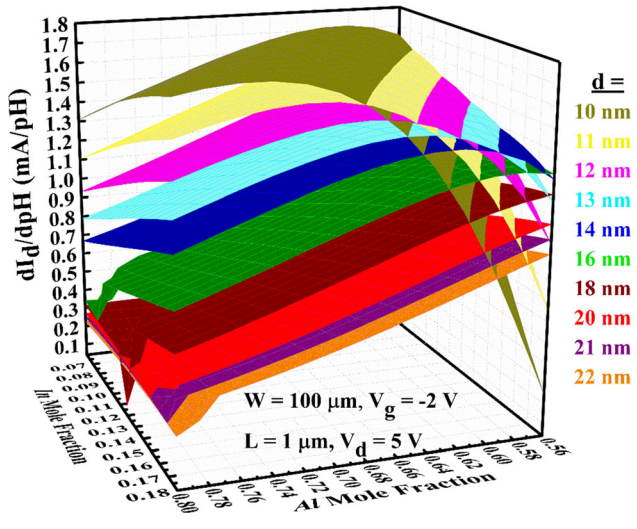

Fig. 19. Sensitivity dI_d/dpH for various mole fractions of Al, In and thickness of barrier layer d, with pH = 7, W = 100 μm, L = 1 μm, V_g = − 2 V and V_d = 5 V.

consistently rise with the W/L ratio. Zhang et al. found that the current sensitivity is limited by the R_{sr} of the packaged sensor.[37]

For the composition dependent analysis, we have calculated the drain current and the sensitivity for drain current as a function of pH with variable mole fractions of In and Al. For this analysis, we have kept the other device parameters constant as W = 100 μm, L = 1 μm, d = 12 nm, V_g = − 2 V and V_d = 5 V. It can be observed from Fig. 16 that for pH levels 4 to 10, the maximum drain current can be achieved with the mole fractions of In = 0.06 and Al = 0.80 for the barrier layer thickness d = 12 nm.

Figure 17 depicts the variation in sensitivity with changing Al and In mole fractions. The maximum sensitivity is calculated as 1.32 mA/pH with In mole fraction 0.16 and Al mole fraction 0.62. We found the sensitivity to be highest for the composition $Al_{0.62}In_{0.16}Ga_{0.22}N$ as compared to the other material compositions at all the pH values. Therefore, this composition can be chosen for a high sensitivity pH sensor with the above mentioned device dimensions.

Along with the composition dependent analysis, we have also analyzed the drain current at different barrier layer thicknesses with variable mole fractions as shown in Figs. 18 and 19. Figure 18 displays that, with thinner barrier layers d = 10 nm to 14 nm, the drain current varies linearly with changing mole fraction, and reaches the maximum value at the mole fraction In = 0.06 and Al = 0.80. When the thickness of the barrier layer increases

from 14 nm to 22 nm, the maximum drain current can be achieved at different mole fractions. Therefore, for the optimized solution, the sensitivity for the drain current is calculated at different barrier thicknesses and variable mole fractions as shown in Fig. 19.

It can be seen that the higher sensitivity is attained for the thinner barrier layers. The highest sensitivity of 1.62 mA/pH at d = 10 nm thickness of the barrier layer is achieved with the composition $In_{0.18}Al_{0.76}GaN$ for pH = 7. Similar analysis can be done for the optimized material composition for other target pH applications.

CONCLUSION

In this paper, we have proposed an In and Al composition dependent unified analytical model for pH sensing applications of InAlGaN/GaN HEMTs. The impact of the change in mole fraction of Al, In and electrolyte pH level on the threshold voltage and the drain current of various device structures has been examined. We have verified that by utilizing suitable In and Al compositions, high concentration of the 2DEG can be obtained in the InAlGaN/GaN heterostructures even with a thin barrier layer. The InAlGaN/GaN devices have slightly higher negative threshold voltage than the conventional AlGaN/GaN HEMTs due to its high 2DEG concentration. The sensitivity of an HEMT based pH sensor is dependent on its transconductance. The maximum transconductance of the AlGaN/GaN devices was found to be much lower than that of the InAlGaN/GaN HEMTs. The thinner barrier layer of the InAlGaN/GaN HEMTs enhance the gate control capability and the transconductance of the device. Increased maximum transconductance in quaternary InAlGaN/GaN leads to enhanced sensitivity to the pH levels of the electrolyte. Therefore, we conclude that exploiting the InAlGaN devices for pH measurement applications can result in better performance. The analytical results show good agreement with the experimental results available in the literature. Average RMSE is found to be miniscule 0.0070. We expect our model to be a useful tool to predict the behavior of HEMTs in different acidic environments and to have applications in device optimization and sensor calibration purposes for future chemical and biochemical sensors. The only shortcoming of this model is to recognize the acceptable approximate values of fitting parameters used.

CONFLICT OF INTEREST

The authors declare that they have no conflict of interest.

REFERENCES

1. L. Manjakkal, D. Szwagierczak, and R. Dahiya, *Prog. Mater. Sci.* 109, 100635 (2020).
2. S. Taheri, *Constr. Build Mater.* 204, 492 (2019).
3. M. Singh, R.S. Patkar, M. Vinchurkarand, and M.S. Baghini, *IEEE Sens. J.* 20, 47 (2019).
4. O. Korostynska, K. Arshak, E. Gill, and A. Arshak, *IEEE Sens. J.* 8, 20 (2007).
5. L. Manjakkal, S. Dervinand, and R. Dahiya (2020) RSC Adv.; 10(15):8594.
6. Q. Cheng, M. Wang, M. Tao, R. Yin, Y. Li, N. Yang, W. Xu, C. Gao, Y. Hao, and Z. Yang, *IEEE Electr. Device L* 41, 485 (2020).
7. M.I. Khan, K. Mukherjee, R. Shoukat, and H. Dong, *Microsyst . Technol.* 23, 4391 (2017).
8. M.T. Ghoneim, A. Nguyen, N. Dereje, J. Huang, G.C. Moore, P.J. Murzynowski, and C. Dagdeviren, *Chem. Rev.* 119, 5248 (2019).
9. C. Zhang, P. Zhang, X. Ma and J. Shi, *2nd International Conference on Frontiers of Sensors Technologies (ICFST)IEEE* (2017), pp. 95-98.
10. S. J. Pearton, F. Ren and B. H. Chu, in *State of the Art in Biosensors: Environmental and Medical Application*s, ed. by Toonika Rinken, (IntechOpen 2013), pp-2287.
11. S.Turuvekere, N. Karumuri, A. Azizur Rahman, A. Bhattacharya, A. D. Gupta, and N. D. Gupta, *IEEE Trans. Electron. Dev.* 60(10), 3157 (2013).
12. M. Stutzmann, G. Steinhoff, M. Eickhoff, O. Ambacher, C. E. Nebel, J. Schalwig, R. Neuberger and G. Müller, *Diam Relat. Mater.* 11(3-6), 886 (2002).
13. R. Mehandru, B. Luo, B.S. Kang, J.H. Kim, F. Ren, S.J. Pearton, and J.I. Chyi, *Solid State Electron.* 48, 351 (2004).
14. T. Kokawa, T. Sato, H. Hasegawa and T. Hashizume, *J. Vac. Sci. Technol. B* 24 (4), 1972 (2006).
15. M.S.Z. Abidin, A.M. Hashim, M.E. Sharifabad, S. Fadzli, A. Rahman, and T. Sadoh, *Sensors* 11, 3067 (2011).
16. J.Y. Pyo, J.H. Jeon, Y. Koh, C.Y. Cho, H.H. Park, K.H. Park, S.W. Lee, and W.J. Cho, *AIP Adv.* 8, 085106 (2018).
17. Y. Dong, D.H. Son, Q. Dai, J.H. Lee, C.H. Won, J.G. Kim, D. Chen, J.H. Lee, H. Lu, R. Zhang, and Y. Zheng, *Sensors* 18, 1314 (2018).
18. I. Sanyal, Y.C. Lee, Y.C. Chen, and J.I. Chyi, *Appl. Phys. Lett.* 114, 222103 (2019).
19. N. M. Shrestha, C. H. Chen, Z. M. Tsai, Y. Li, J. H. Tarng and S. Samukawa, in *IEEE International Conference on Simulation of Semiconductor Processes and Devices (SISPAD)*, (2019), pp 1-4.
20. F.G. McIntosh, K.S. Boutros, J.C. Roberts, S.M. Bedair, E.L. Piner, and N.A. El Masry, *Appl. Phys. Lett.* 68, 40 (1996).
21. E.L. Piner, F.G. McIntosh, J.C. Roberts, M.E. Aumer, V.A. Joshkin, S.M. Bedair, and N.A. El-Masry, *MRS Internet J N S R* 1, 43 (1996).
22. N. Ketteniss, L. Rahimzadeh Khoshroo, M. Eickelkamp, M. Heuken, H. Kalisch, R.H. Jansen, and A. Vescan (2010) *Semicond. Sci. Technol.*; 25(7): 075013.
23. J.H. Hwang, S.M. Kim, J.M. Woo, S.M. Hong, and J.H. Jang, *Phys. Status Solidi A* 213, 889 (2016).
24. E. Dogmus, R. Kabouche, S. Lepilliet, A. Linge, M. Zegaoui, H. Ben-Ammar, M.P. Chauvat, P. Ruterana, P. Gamarra, C. Lacam, and M. Tordjman, *Electronics* 5, 31 (2016).
25. L. Ravi, and B. Krishnan, *Optik* 178, 66 (2019).
26. A. Minj, D. Skuridina, D. Cavalcoli, A. Cros, P. Vogt, M. Kneissl, C. Giesen, and M. Heuken, *Mater. Sci. Semicond. Process.* 55, 26 (2016).
27. M. Bayer, C. Uhl, and P. Vogl, *J. Appl. Phys.* 97, 033703 (2005).
28. M. Sciullo, M. Choudhury, E. Patrick, and M.E. Law, *ECS Trans.* 75, 259 (2016).
29. S. Rabbaa, and J. Stiens, *J. Phys. D Appl. Phys.* 45, 475101 (2012).
30. R. Anvari, D. Spagnoli, G.A. Umana-Membreno, G. Parish, and B. Nener, *Appl. Surf. Sci.* 452, 75 (2018).
31. D. Godwinraj, H. Pardeshi, S.K. Pati, N. Mohankumar, and C.K. Sarkar, *Superlattices Microstruct.* 54, 188 (2013).
32. H.R. Mojaver, F. Manouchehri, and P. Valizadeh, *J. Appl. Phys.* 119, 154502 (2016).
33. Y. Li, J. Zhang, W. Wan, Y. Zhang, Y. Nie, J. Zhang, and Y. Hao, *Physica E* 67, 77 (2015).

34. Y. Li, J. Zhang, G. Liu, R. Quan, X. Duan, J. Zhang, and Y. Hao, *AIP Adv.* 7, 105109 (2017).
35. K.T. Upadhyay, and M.K. Chattopadhyay, *Mater. Today-Proc.* 19, 205 (2019).
36. G. Parish, F.L.M Khir, N... Radha Krishnan, J. Wang, J.S. Krisjanto, H. Li, G.A. Umana-Membreno, S. Keller, UK Mishra, M.V. Baker, B.D. Nener, and M. Myers (2019) *Sensor Actuat B-Chem.* 287, 250 (2019).
37. H. Zhang, J. Tu, S. Yang, K. Sheng, and P. Wang, *Talanta* 205, 120134 (2019).
38. P. Murugapandiyan, A. Mohanbabu, V.R. Lakshmi, M. Wasim, and M. Sundaram, *Journal of Elec Materi* 49, 524 (2020).
39. F.M. Yigletu, S. Khandelwal, T.A. Fjeldly, and I. Benjamín, *IEEE Trans. Electron Devices* 60, 3746 (2013).
40. N.S. Swamy, and A.K. Dutta, *IEEE T Electron Dev.* 65, 936 (2018).
41. R. Narang, M. Saxena, and M. Gupta, *IEEE Trans. Electron Devices* 64, 1742 (2017).
42. Y. Xu, and M.A. Schoonen, *Am. Mineral.* 85, 543 (2000).
43. M. Kosmulski, *J Colloid Interface Sci.* 238, 225 (2001).
44. K.T. Upadhyay, and M.K. Chattopadhyay, *Mater. Scie. Eng.: B*, 263, 114849 (2021).